Electric Field-Induced Instability in a Non-Newtonian Hybrid Nanofluid

V. Sharma[a], J. Devi[b], V. Sharma[b] and G.C. Rana[c,*]

[a]*Department of Mathematics, Govt. College, Tissa, Chamba, Himachal Pradesh-176316, India*
[b]*Department of Mathematics and Statistics, Himachal Pradesh University, Summer Hill, Shimla-171005, India*
[c]*Principal, Government Degree College, Dhaneta, Himachal Pradesh-177041, India*

Received: 19.08.2025 & Accepted: 07.11.2025

Doi: 10.12693/APhysPolA.148.318 *e-mail: drgcrana15@gmail.com

The influence of fluid rheology on the onset of thermal convection in a hybrid nanofluid layer subjected to a vertical alternating current electric field is investigated using linear stability theory with stress-free boundary conditions. The analysis incorporates the Buongiorno model for nanoparticle transport and the Maxwell model to describe non-Newtonian rheology, accounting for both thermophoresis and Brownian motion effects. Hybrid nanofluids — engineered by dispersing dissimilar nanoparticles in a base fluid — exhibit enhanced thermal conductivity and complex flow behaviour. An eigenvalue problem governing the onset of convection is formulated and solved analytically using a single-term Galerkin method, resulting in exact expressions for the critical thermal Rayleigh number for both bottom–heavy and top–heavy configurations. The comparative stability behaviour of ordinary nanofluids and hybrid nanofluids is examined, with articular emphasis on the enhancement of thermal transport properties. The effects of key dimensionless parameters — such as the Lewis number, nanoparticle Rayleigh number, electric Rayleigh number, and the modified diffusivity ratio — on the threshold for stationary convection are analysed both analytically and numerically. These values are numerically computed using software Mathematica 12. Results reveal the significant role of rheology and electric fields in modulating the convective stability of hybrid nanofluids, offering insights for thermal management in advanced electrohydrodynamic systems.

topics: Maxwell model, hybrid nanofluid, alternating current (AC) electric field, thermal convection

1. Introduction

The interaction between thermal and electrohydrodynamic (EHD) processes has been widely explored through experiments involving dielectric fluids exposed to external electric fields. This approach is crucial for improving heat transfer efficiency and evaluating system stability. Incorporating electric fields into thermal systems offers significant advantages, such as reduced energy consumption, lower operational costs, and enhanced performance. Numerous studies have investigated the effects of electric fields on natural convection in dielectric fluids, where spatial variations in permittivity and electrical conductivity give rise to electroconvection — a phenomenon comparable to Bénard convection [1]. This occurs when a horizontally extended fluid layer experiences both gravitational forces and an alternating current (AC) electric field, with electroconvection emerging due to the interplay between thermal buoyancy and electric body forces.

A considerable number of analytical and experimental efforts have focused on the stability of dielectric fluid layers under the influence of an electric field. While classical thermal convection is commonly associated with bottom-heated configurations, instances of convection have also been reported when the fluid layer is heated from above in the presence of a uniform electric field [2]. Further developments include investigations incorporating temperature-dependent dielectric constants [3], as well as the combined effects of weak unipolar injection and thermal gradients on stability behavior [4]. Expanding upon these findings, several comprehensive studies have provided deeper insights into the governing mechanisms and conditions for electroconvection [5–9].

Nanofluids, formulated by dispersing nanoscale particles such as metal oxides, carbides, nitrides, pure metals, or carbon-based structures (e.g. nanotubes), into conventional base fluids like water or ethylene glycol, have demonstrated considerable enhancements in thermal conductivity [10].

These advanced fluids are utilized in a variety of fields, including nanocomposites, enhanced oil recovery systems, pharmaceutical formulations, and efficient thermal management systems. Commonly used nanoparticles such as Al_2O_3, CuO, ZnO, and TiO_2 possess distinct thermal and optical properties that contribute to nanofluid performance. Early theoretical work on predicting thermal conductivity in colloidal dispersions was presented in [11]. Computational strategies (including the lattice Boltzmann method) have been adopted to examine heat transfer mechanisms in nanofluids [12].

An influential model, incorporating effects like Brownian motion and thermophoretic diffusion, was introduced to analyze the thermal instability in such fluids [13], and this framework has been extended to investigate convective phenomena in various thermal environments [14, 15]. Research has also been conducted into electrothermal convection in dielectric nanofluids, focusing on the influence of parameters such as cell geometry and the AC electric Rayleigh–Darcy number [16]. Additionally, the role of electric fields in modifying the thermal performance of nanofluids inside grooved heat pipe systems under steady-state heating conditions has been explored [17].

Numerous investigations have focused on understanding how various parameters influence the thermal performance of hybrid nanofluids. Reviews of entropy generation in these fluids have emphasized their potential to enhance thermal system efficiency [18]. Improved heat transfer, attributed to the combined effects of different nanoparticles, has been reported in flow scenarios involving step-shaped geometries [19]. The stability characteristics of horizontal nano-liquid layers have been explored, with attention to the roles of nanoparticle distribution and buoyancy-driven coupling. These studies indicate that thermo-nanofluid Lewis numbers can destabilize convection when heavier particles accumulate near the top surface, while they have a stabilizing effect when located near the bottom. In both configurations, the concentration Rayleigh number acts to promote convective motion [20].

Further research has investigated the effects of electromagnetic fields on the flow and thermal transport characteristics of hybrid nanofluids, revealing notable influences on the system behavior [21]. Studies involving solutal gradients and thermal loading have demonstrated enhanced convective responses in systems where particles are concentrated near the upper boundary [22]. Comparative evaluations of different thermal conductivity models have shown that mechanisms such as nanoparticle clustering and the formation of interfacial nano-layers contribute to improved heat conduction, especially in specific nanofluid formulations [23].

Non-Newtonian fluids are characterized by a nonlinear relationship between shear stress and shear rate, resulting in complex flow behaviors that significantly impact heat transfer efficiency and the onset of convective instabilities. Among the various rheological models, Maxwell fluids are of particular interest due to their viscoelastic properties, which vary with time. Recent research has explored the thermal performance of hybrid nanofluids incorporating non-Newtonian base fluids, showing notable improvements in both heat transfer and flow stability. Studies indicate that the inclusion of hybrid nanoparticles enhances thermal transport, and that a higher volume fraction of nanoparticles can amplify these improvements.

Investigations focussing on electrothermal convection in dielectric nanofluids governed by Maxwell-type rheology have identified oscillatory patterns in both top–heavy and bottom–heavy particle distributions. The presence of an electric field has been shown to lower the critical Rayleigh number, thereby promoting the earlier onset of instability [24]. Comparable behaviors have also been documented in other non-Newtonian models, such as Oldroyd fluids, where the interplay between rheological properties and electric forces leads to accelerated instability development [25].

Recent advancements in fluid mechanics continue to drive interest in hybrid nanofluids, particularly those formulated from non-Newtonian base fluids, due to their enhanced thermal transport and tailored viscous behavior. A notable computational investigation examined bio-convective magnetohydrodynamic flow of a hybrid nanofluid within a non-Newtonian medium over both conical and flat geometries, integrating refined models that incorporate thermal and solutal relaxation times for improved accuracy in describing energy and mass transport in complex systems [26–29]. In parallel, studies on tri-hybrid nanofluid systems applied to solar-powered residential technologies have underscored the role of entropy minimization in achieving optimal energy utilization [30]. Furthermore, boundary layer flow analyses of non-Newtonian hybrid nanofluids past horizontal cylinders have shown that increasing the concentrations of nanoparticles, such as titanium oxide (TiO_2) and copper oxide (CuO), enhances the thermal boundary layer thickness and boosts the energy transfer rates [31].

Building upon these developments, the current study focuses on examining the onset of thermal convection in a hybrid nanofluid layer characterized by Maxwell-type rheology under the influence of an alternating electric field. Unlike prior studies, which largely overlook the combined effects of rheology, electric fields, and nanoparticle synergy in such configurations, this work aims to fill this gap. Specifically, it investigates the thermal stability of a hybrid nanofluid layer heated from below, providing a detailed analysis that incorporates essential physical and thermodynamic interactions previously unexplored in the literature.

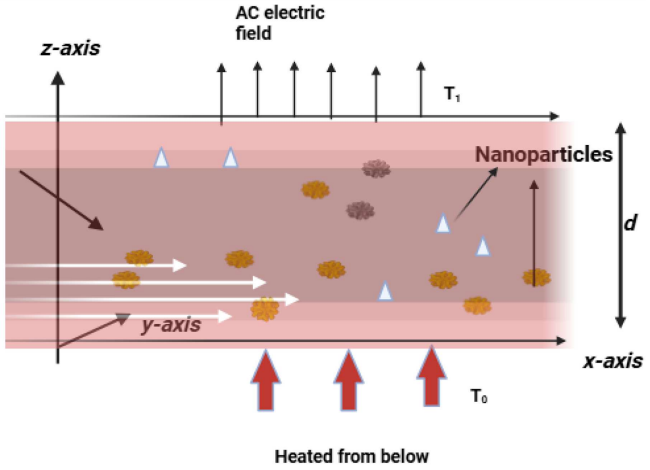

Fig. 1. Geometric configuration of the system.

2. Mathematical formulation

Consider an incompressible, electrically conductive, horizontal layer of a hybrid nanofluid that is modelled as a Maxwell-type viscoelastic fluid. This layer is bounded between two infinite, parallel planes spaced by a distance d. The lower boundary is uniformly heated, and both the temperature and volume fraction distributions of hybrid nanoparticles at the boundaries are T_0 and ϕ_{10}, ϕ_{20} at $z = 0$ and T_1 and ϕ_{21} at $z = d$, respectively, as shown in Fig. 1.

The nanoparticle distribution along the vertical direction is generally non-uniform due to Brownian motion and thermophoresis, which alter the local density profile and the buoyancy forces that drive convection. In the present study, a hybrid nanofluid layer is considered with such a non-uniform nanoparticle distribution, specifically examining the bottom–heavy condition ($\phi_{10} > \phi_{11}$ and $\phi_{20} > \phi_{21}$), where the lower region has a higher particle fraction of the two types of nanoparticles, and the top–heavy condition ($\phi_{11} < \phi_{10}$ and $\phi_{20} < \phi_{21}$), where the upper region has a higher particle fraction of the same two nanoparticle types. These configurations form the basis for subsequent analysis.

The physical system under consideration is subjected to gravitational acceleration $\boldsymbol{g} = (0, 0, -g)$ and a uniform alternating current (AC) electric field, both aligned along the vertical z axis. The lower boundary is electrically connected to a circuit, while the upper boundary maintains a root mean square (RMS) electric potential, φ. For the sake of analytical tractability, all thermophysical properties are treated as constant, with the exception of fluid density, which may vary with temperature and concentration.

The present study develops a generalized electrohydrodynamic convection model for hybrid nanofluids by extending the conventional viscoelastic framework. The current analysis adopts the Maxwell viscoelastic model, which retains only the dominant relaxation mechanism and is more suitable for moderate relaxation times and weak retardation behaviour. Accordingly, the momentum equation is modified by applying the Maxwell operator $(1 + \overline{\lambda}_1 \frac{\partial}{\partial t})$ to both the inertial and stress terms. This refinement simplifies the rheological structure of the model while preserving the essential elastic nature of the flow.

In addition, the nanoparticle concentration and energy balance equations were extended to account for two nanoparticle components, thereby capturing both the Brownian diffusion and thermophoretic transport phenomena. These modifications provide a more comprehensive and physically consistent representation of hybrid nanofluid convection under the influence of electrohydrodynamic. The governing conservation equations for the mass, momentum, nanoparticle concentration, and energy (after incorporating the changes and modifications) take the following generalized form ([13, 22, 24, 32, 33]), respectively,

$$\nabla \cdot \boldsymbol{v} = 0, \tag{1}$$

$$\rho_f \left(1+\overline{\lambda}_1 \frac{\partial}{\partial t}\right) \left[\frac{\partial \boldsymbol{v}}{\partial t} + (\boldsymbol{v} \cdot \nabla)\, \boldsymbol{v}\right] = \left(1+\overline{\lambda}_1 \frac{\partial}{\partial t}\right) (-\nabla P - f_e) + \mu \nabla^2 \boldsymbol{v} + \left(1+\overline{\lambda}_1 \frac{\partial}{\partial t}\right) \Big[\phi_1 \rho_{p_1} + \phi_2 \rho_{p_2} + (1-\phi_1-\phi_2)\, \rho_f \Big(1 - \beta\,(T-T_0)\Big)\Big] \boldsymbol{g}, \tag{2}$$

$$\left[\frac{\partial \boldsymbol{v}}{\partial t} + (\boldsymbol{v}\cdot\nabla)\,\boldsymbol{v}\right]\phi_1 = D_{B_1}\nabla^2\phi_1 + \frac{D_{T_1}}{T_0}\nabla^2 T, \tag{3}$$

$$\left[\frac{\partial \boldsymbol{v}}{\partial t} + (\boldsymbol{v}\cdot\nabla)\,\boldsymbol{v}\right]\phi_2 = D_{B_2}\nabla^2\phi_2 + \frac{D_{T_2}}{T_0}\nabla^2 T, \tag{4}$$

and

$$(\rho c)_f\left[\frac{\partial}{\partial t} + (\boldsymbol{v}\cdot\nabla)\right]T = (\rho c)_{p_1}\left[D_{B_1}(\nabla\phi_1)\cdot(\nabla T) + \frac{D_{T_1}}{T_0}(\nabla T)\cdot(\nabla T)\right] + (\rho c)_{p_2}\Big[D_{B_2}\,(\nabla\phi_2)\cdot(\nabla T) + \frac{D_{T_2}}{T_0}\,(\nabla T)\cdot(\nabla T)\Big] + k_f\nabla^2 T, \tag{5}$$

where $\boldsymbol{v} = (u, v, w)$, μ, ρ_f, p, T, β, and g denote fluid velocity, viscosity coefficient, base fluid density, pressure, temperature, adverse temperature gradient, and gravitational acceleration, respectively. Furthermore, ρ_{p_1} and ρ_{p_2} denote the densities of hybrid nanoparticles; $(\rho c)_f$ and $(\rho c)_{p_1}$ as well $(\rho c)_{p_2}$ are the heat capacity of the fluid and hybrid nanoparticles, respectively; ϕ_1 and ϕ_2 are the volume fraction of hybrid nanopartcles; $\overline{\lambda}_1$ is the stress relaxation; D_{T_1}, D_{T_2} and D_{B_1}, D_{B_2} are the thermophoretic coefficients and Brownian diffusion coefficients of hybrid nanoparticles, respectively; and k_f is the thermal conductivity.

The parameters P and f_e in (2) represent the modified pressure and electric origin force, respectively, and they are expressed as

$$P = p + \frac{\rho_f}{2}\left(\frac{\partial\gamma}{\partial t}\right)E^2 \tag{6}$$

and

$$f_e = \rho_e E - \frac{1}{2}E^2\,\nabla\gamma + \frac{1}{2}\nabla\left(\rho_f\frac{\partial\gamma}{\partial t}E^2\right), \tag{7}$$

where ρ_e, γ and E represent the charged particles density, dielectric constant and electric field, respectively. Regarding the dielectric constant and fluid density, these can be described as

$$\gamma = \gamma_0{}'\Big[1 - e_0\,(T - T_0)\Big],$$
$$\rho_f = \rho_0\Big[1 - \alpha\,(T - T_0)\Big], \tag{8}$$

where $e_0 > 0$ denotes the dielectric constant coefficient with very small relative temperature variations, and α and ρ_0 represent the volume expansion coefficient and the fluid density in the lower layers, respectively.

When an AC electric field is applied to a hybrid nanofluid, the suspended charged nanoparticles experience an electrohydrodynamic force that drives them along the electric field lines, thereby transferring momentum to the surrounding base fluid. This interaction gives rise to a coupled electrostatic–hydrodynamic behaviour, which governs the overall flow and transport processes in the hybrid nanofluid. The electric field distribution in such a system is by Maxwell's electrostatic equations, which for a dielectric hybrid nanofluid are expressed as

$$\nabla\cdot(\gamma\,\boldsymbol{E}) = 0, \qquad \nabla\times\boldsymbol{E} = 0. \tag{9}$$

The electric field is derived from the scalar potential φ, represented by $\boldsymbol{E} = -\nabla\varphi$. Using this relation in (9), one gets

$$\nabla^2\varphi = 0, \tag{10}$$

where φ denotes the electric potential (root mean square value). Note that (9) and (10) retain the same mathematical form for both nanofluids and hybrid nanofluids. This is because Maxwell's field equations describe the fundamental electrostatic behaviour of dielectric media and are independent of the specific fluid composition. The influence of hybridization appears only through the effective material properties, such as permittivity, conductivity, and viscosity, rather than through any modification of the governing electrostatic equations. Retaining this conventional formulation ensures consistency with the electrohydrodynamic framework and accurately captures the coupling between the electric field distribution and fluid motion in the hybrid nanofluid system. The relevant boundary conditions, when $z = 0$ and $z = d$, are

$$w = T = \phi_1 = \phi_2 = \frac{\partial^2 w}{\partial z^2} = \frac{\partial\varphi}{\partial z} = 0. \tag{11}$$

By introducing the following dimensionless variables

$$(u, v, w)\,\alpha_m = (u^*, v^*, w^*)\,,$$
$$(x, y, z)\,d = (x^*, y^*, z^*)\,,$$
$$\frac{t\,d^2}{\alpha_m} = t^*, \qquad p\frac{(\mu\alpha_m)}{d^2} = p^*, \qquad \frac{\varphi}{eE_0\beta d} = \varphi^*,$$
$$\phi_1^* = \frac{\phi_1 - \phi_{10}}{\phi_{10}}, \qquad \phi_2^* = \frac{\phi_2 - \phi_{20}}{\phi_{20}},$$
$$T = \frac{T^* - T_1}{T_0 - T_1}, \qquad \alpha_m = \frac{k_f}{(\rho c)_f}, \tag{12}$$

in the partial differential equations (2)–(5) and (10), after using (12), the dimensionless form (dropping asterisks for simplicity) of the equations is obtained

$$\nabla\cdot\boldsymbol{v} = 0, \tag{13}$$

$$\frac{1}{P_r}\Big(1+\lambda_1\frac{\partial}{\partial t}\Big)\frac{\partial \boldsymbol{v}}{\partial t} = \Big(1+\lambda_1\frac{\partial}{\partial t}\Big)\Big[R_e\Big(T-\frac{\partial \varphi}{\partial z}\Big)+R_aT-R_m-\nabla P\Big] - \Big(1+\lambda_1\frac{\partial}{\partial t}\Big)\Big[R_{n_1}\phi_1+R_{n_2}\phi_2\Big]+\nabla^2\boldsymbol{v}, \tag{14}$$

$$\frac{\partial T}{\partial t}+(\boldsymbol{v}\cdot\nabla)\,T=\nabla^2T+\frac{N_{B_1}}{L_{n_1}}\big((\nabla T)\cdot(\nabla\phi_1)\big) + \frac{2N_{A_1}N_{B_1}}{L_{n_1}}\,(\nabla T)^2+\frac{N_{B_2}}{L_{n_2}}\,((\nabla T)\cdot(\nabla\phi_2)) + \frac{2N_{A_2}N_{B_2}}{L_{n_2}}\,(\nabla T)^2, \tag{15}$$

$$\frac{\partial \phi_1}{\partial t}+(\boldsymbol{v}\cdot\nabla)\,\phi_1=\frac{1}{L_{n_1}}\nabla\cdot(\nabla\phi_1)+\frac{N_{A_1}}{L_{n_1}}\,\nabla\cdot(\nabla T), \tag{16}$$

$$\frac{\partial \phi_2}{\partial t}+(\boldsymbol{v}\cdot\nabla)\,\phi_2=\frac{1}{L_{n_2}}\nabla\cdot(\nabla\phi_2)+\frac{N_{A_2}}{L_{n_2}}\,\nabla\cdot(\nabla T), \tag{17}$$

$$\boldsymbol{E}=-\nabla\varphi, \tag{18}$$

with the following dimensionless parameters:

- thermal Prandtl number $P_r{=}\mu/(\rho_0\alpha)$,
- Rayleigh number due to electric field $R_e{=}\gamma_0\, e_0^2E_0^2\beta^2d^2/(\mu\,\alpha_m)$,
- basic density-Rayleigh number $R_m{=}gd^3[\phi_{10}\,\rho_{P_1}{+}\phi_{20}\,\rho_{P_2}{+}\rho_f(1{-}\phi_{10}{-}\phi_{20})]/(\mu\,\alpha_m)$,
- thermal Rayleigh number $R_a{=}\alpha\,\rho_f\,g\,d^3\Delta T/(\mu\alpha_m)$,
- stress-relaxation time $\lambda_1{=}\overline{\lambda}_1\,\alpha/d^2$.

In the paper, $\nabla_1^2=(\frac{\partial^2}{\partial x^2}+\frac{\partial^2}{\partial y^2})$ and $\nabla^2=(\frac{\partial^2}{\partial x^2}+\frac{\partial^2}{\partial y^2}+\frac{\partial^2}{\partial z^2})$ are two- and three-dimensional Laplacian operators, respectively.

In the case of hybrid nanofluids, the presence of two or more types of nanoparticles introduces additional non-dimensional parameters to account for their combined influence on convective transport and stability. These parameters are:

- hybrid nanofluid Lewis numbers $L_{n_1}{=}\alpha_m/D_{B_1}$ and $L_{n_2}{=}\alpha_m/D_{B_2}$,
- increments in the particle density $N_{B_1}{=}(\rho c)_{P_1}(\phi_{11}{-}\phi_{10})(\rho c)_f{}^{-1}$ and $N_{B_2}{=}(\rho c)_{P_2}(\phi_{21}{-}\phi_{20})(\rho c)_f{}^{-1}$,
- concentration Rayleigh numbers $R_{n_1}{=}(\rho_{p_1}{-}\rho_{f0})(\phi_{11}{-}\phi_{10})gd^3/(\mu\,\alpha)$ and $R_{n_2}{=}(\rho_{p_2}{-}\rho_{f0})(\phi_{21}-\phi_{20})gd^3/(\mu\,\alpha)$,
- modified diffusivity ratios $N_{A_1}{=}D_{T_1}(T_0-T_1)/[D_{B_1}T_0(\phi_{11}-\phi_{10})]$ and $N_{A_2}{=}D_{T_2}(T_0-T_1)/[D_{B_2}T_0(\phi_{2_1}-\phi_{2_0})]$.

These parameters collectively capture the influence of each nanoparticle type on density stratification, buoyancy forces, and the onset of convection in the hybrid nanofluid.

3. Primary flow and disturbed equations

The base state of the system is considered to be quiescent and steady, with no time dependence and negligible sedimentation of suspended nanoparticles. Under these conditions, temperature, pressure, electric field, dielectric constant, and electric potential are assumed to vary solely in the vertical direction. The solutions for this base state, derived from (13 –(18), are given respectively by

$$\begin{aligned} &v=v_b=0, \qquad T=T_b\,(z)=T_0-\beta z,\\ &\phi_1=\phi_{1b}, \qquad \phi_2=\phi_{2b}, \qquad p=p_b\,(z)\,,\\ &\varphi=-E_0\log\,(1+e_0\beta\,z)/(e_0\beta)=\varphi_b\,(z)\,,\\ &\gamma=\gamma_0\,(1+e\beta z)=\gamma_b\,(z)\,,\\ &E=E_0/(1+e_0\,\beta z)=E_b\,(z)\,, \end{aligned} \tag{19}$$

where $\beta=(T_0{-}T_1)/d$ and $E_0 = -\varphi_1\,e_0\,\beta z/\log(1{+}e_0\beta z)$ represent the adverse thermal gradient andelectric field (root mean square value) at $z=0$ and subscript 'b' indicates basic state. The basic (primary) flow profile is similar for all considered fluids, including single-component nanofluids and hybrid nanofluids. However, in the case of hybrid nanofluids, the volume fractions of the individual nanoparticles (ϕ_1,ϕ_2) differ, leading to modifications in the effective density and thermal properties of the base layer. These differences in nanoparticle concentrations affect the density stratification and buoyancy forces, thereby influencing the onset of convection.

Infinitesimal perturbations are superimposed to the fundamental (basic) state flow in order to check the system stability, taken as

$$\begin{aligned} &\boldsymbol{v}=\boldsymbol{v}', \qquad T=T_b+T',\\ &\phi_1=\phi_{1b}+\phi'_1, \qquad \phi_2=\phi_{2b}+\phi'_2,\\ &p=p_b+p', \qquad \gamma=\gamma_0+\gamma',\\ &\varphi_1=\varphi_{1b}+\varphi'_1, \qquad \boldsymbol{E}=\boldsymbol{E}+\boldsymbol{E}' \end{aligned} \tag{20}$$

where $\boldsymbol{v}'$, ϕ'_1, ϕ'_2, T', p', $\boldsymbol{E}'$, γ'_1 and φ'_1 denote the disturbed physical quantities.

Substituting the perturbation expressions from (20) into the governing relations, and using (19) in conjunction with (13)–(18), while neglecting nonlinear terms arising from products of perturbations and eliminating the pressure variable, yields the simplified linearized non-dimensional equations

$$\frac{1}{P_r}\Big(1+\lambda_1\frac{\partial}{\partial t}\Big)\frac{\partial}{\partial t}\Big(\nabla^2w'\Big) = \Big(1+\lambda_1\frac{\partial}{\partial t}\Big)\Big[R_e\nabla_1^2\Big(T'-\frac{\partial\varphi'}{\partial z}\Big)+R_a\nabla_1^2T'\Big] - \Big(1+\lambda_1\frac{\partial}{\partial t}\Big)\Big[R_{n_1}\nabla_1^2\phi'_1+R_{n_2}\nabla_1^2\phi'_2\Big] + \big(\nabla^4w'\big) \tag{21}$$

$$\frac{\partial T'}{\partial t} - w' = \nabla^2 T' + \frac{N_{B_1}}{L_{n_1}}\left(\frac{\partial T'}{\partial z} - \frac{\partial \phi_1{}'}{\partial t}\right) - \frac{2N_{A_1}N_{B_1}}{L_{n_1}}\frac{\partial T'}{\partial z} + \frac{N_{B_2}}{L_{n_2}}\left(\frac{\partial T'}{\partial z} - \frac{\partial \phi_2{}'}{\partial t}\right) - \frac{2N_{A_2}N_{B_2}}{L_{n_2}}\frac{\partial T'}{\partial z}, \tag{22}$$

$$\frac{\partial \phi_1{}'}{\partial t} + w' = \frac{1}{L_{n_1}}\nabla^2 \phi_1{}' + \frac{N_{B_1}}{L_{n_1}}\nabla^2 T', \tag{23}$$

$$\frac{\partial \phi_2{}'}{\partial t} + w' = \frac{1}{L_{n_2}}\nabla^2 \phi_2{}' + \frac{N_{B_2}}{L_{n_2}}\nabla^2 T', \tag{24}$$

$$\nabla^2 \varphi' + e\,E_0 \frac{\partial T'}{\partial z} = 0, \tag{25}$$

4. Normal mode method

The solution to the coupled differential equations (21)–(25) is obtained by representing the perturbed physical quantities as normal modes. This can be described in the following form

$$(w', T', \Phi', \varphi') = [W(z), \Theta(z), \Phi(z), \Psi(z)]\ \mathrm{e}^{\sigma t + \mathrm{i}(k_x x + k_y y)}. \tag{26}$$

Here, k_x and k_y represent the perturbation wave numbers along the x and y axes, respectively, while σ denotes the complex growth rate. The wave number corresponding to the solution is represented by $a = \sqrt{k_x^2 + k_x^2}$.

Using (26) in (21)–(25), we get a set of linearized ordinary differential equations, namely

$$\left(D^2-a^2\right)\left[\left(D^2-a^2\right) - \frac{\sigma}{P_r}(1+\lambda_1\sigma)\right]^2 W - \left[\left(D^2-a^2\right) - \frac{\sigma}{P_r}(1+\lambda_1\sigma)\right] a^2\left[(R_a+R_e)\Theta - (R_{n_1}\Phi_1 + R_{n_2}\Phi_2) + R_e D\Psi\right] = 0, \tag{29}$$

$$W + \left[\left(D^2-a^2-\sigma\right) + \frac{N_{B_1}}{L_{n_1}}D + \frac{N_{B_2}}{L_{n_2}}D - \frac{2N_{A_1}N_{B_1}}{L_{n_1}} - \frac{2N_{A_2}N_{B_2}}{L_{n_2}}\right]\Theta - \left(\frac{N_{B_1}}{L_{n_1}} + \frac{N_{B_2}}{L_{n_2}}\right)D\Psi = 0, \tag{28}$$

$$W - \frac{N_{A_1}}{L_{n_1}}\left(D^2-a^2\right)\Theta - \left[\frac{1}{L_{n_1}}\left(D^2-a^2\right) + \sigma\right]\Phi_2 = 0, \tag{29}$$

$$W - \frac{N_{A_2}}{L_{n_2}}\left(D^2-a^2\right)\Theta - \left[\frac{1}{L_{n_2}}\left(D^2-a^2\right) + \sigma\right]\Phi_2 = 0, \tag{30}$$

$$\left(D^2 - a^2\right)\Psi + D\Theta = 0. \tag{31}$$

Here, $D = \mathrm{d}/\mathrm{d}z$ denotes differentiation with respect to the vertical coordinate. After utilizing (26), the boundaries (11) (at $z = 0$ and $z = 1$) yield

$$W = D^2 W = \Theta = \Phi_1 = \Phi_2 = D\Psi = 0. \tag{32}$$

5. Method of solution

The Galerkin weighted residuals method (GWRM) is applied to evaluate approximate solutions of the ordinary differential equations (27)–(31) satisfying the boundary conditions (32). The choice of trial function $(W, \Theta, \Phi_1, \Phi_2, \Psi)$ depends on the the type of boundary conditions. For these functions, we postulate the following form

$$W = \sum_{j=1}^{M} A_j W_j, \qquad \Theta = \sum_{j=1}^{M} B_j \Theta_j,$$
$$\Phi_1 = \sum_{j=1}^{M} C_{j1}\Phi_{1j}, \quad \Phi_2 = \sum_{j=1}^{M} C_{j2}\Phi_{2j},$$
$$\Psi = \sum_{j=1}^{M} D_j \Psi_j, \tag{33}$$

where $A_j, B_j, C_{j1}, C_{j2}, D_j$ (for $j = 1, 2, M$) are constants (unknown). Using (33) in (27)–(31) and multiplying the equations by W_j, Θ_j, Φ_{1j}, Φ_{2j}, Ψ_j, respectively, and then integrating them between the limits 0 and 1 (i.e., $0 < z < 1$) with the use of the boundary conditions (32), a system of $4M$ homogeneous equations with $4M$ unknowns $A_j, B_j, C_{j1}, C_{j2}, D_j$ is obtained. Using the condition of orthogonality and making the determinant of the coefficient matrix of the system of equations equal zero for non-trivial solutions, we obtain the characteristic equation with the thermal Rayleigh number as eigen value.

For $M = 1$, the exact solutions of (27)–(31) using the GWRM satisfying boundary conditions (32) are taken as

$$W = A_1 \sin(\pi z), \qquad \Theta = B_1 \sin(\pi z),$$
$$\Phi_1 = C_1 \sin(\pi z), \qquad \Phi_2 = C'_1 \sin(\pi z),$$
$$\Psi = D_1 \cos(\pi z). \tag{34}$$

Using the solutions (34) in (27)–(31) and applying the boundary conditions given in (32), the following matrix is obtained

$$\begin{pmatrix} (J^2+\frac{\sigma}{p_r}JK_1) & -a^2(R_a+R_e)K_1 & a^2R_{n_1}K_1 & a^2R_{n_2}K_1 & -R_ea^2\pi K_1 \\ 1 & -J-\sigma & 0 & 0 & 0 \\ 1 & \frac{N_{A_1}}{L_{n_1}}J & \frac{J}{L_{n_1}}+\sigma & 0 & 0 \\ 1 & \frac{N_{A_2}}{L_{n_2}}J & 0 & \frac{J}{L_{n_2}}+\sigma & 0 \\ 0 & -\pi & 0 & 0 & -J \end{pmatrix} \begin{pmatrix} A_1 \\ B_1 \\ C_1 \\ C_1' \\ D_1 \end{pmatrix} = 0, \tag{35}$$

where $J=(a^2+\pi^2)$, $K_1=(1+\lambda_1\sigma)$. From (35) one can obtain

$$R_a = \frac{J\sigma(J+\sigma)}{a^2p_r} + \frac{(-J+\pi^2)\sigma^2L_{n_1}L_{n_2}R_e}{J(J+\sigma L_{n_1})(J+\sigma L_{n_2})} + \frac{\left(-J+\pi^2\right)\left[J+\sigma\left(L_{n_1}+L_{n_2}\right)\right]R_e}{\left(J+\sigma L_{n_1}\right)\left(J+\sigma L_{n_2}\right)} + \frac{J^2\left(J+\sigma\right)}{a^2\left(1+\sigma\lambda_1\right)}$$
$$-\frac{\left(J+\sigma L_{n_2}\right)\left[\left(J+\sigma\right)L_{n_1}+JN_{A_1}\right]R_{n_1}}{\left(J+\sigma L_{n_1}\right)\left(J+\sigma L_{n_2}\right)} - \frac{\left(J+\sigma L_{n_1}\right)\left[\left(J+\sigma\right)L_{n_2}+JN_{A_2}\right]R_{n_2}}{\left(J+\sigma L_{n_1}\right)\left(J+\sigma L_{n_2}\right)}. \tag{36}$$

Equation (36) provides a comprehensive framework to predict the critical conditions for the onset of convection in hybrid nanofluid layers under an applied electric field.

6. Mathematical analysis

6.1. Oscillatory convection

The convection through pure oscillatory modes is characterized by taking real part of σ zero. Then putting $\sigma = \mathrm{i}\omega$ in (36) and after some mathematical simplifications, we get

$$R_a = \Delta_1 + \mathrm{i}\omega\Delta_2, \tag{37}$$

where

$$\Delta_1 = -\frac{J\omega^2}{a^2p_r} + \frac{(-J+\pi^2)}{J}R_e + \frac{J^2(J+\omega^2\lambda_1)}{a^2(1+\omega^2\lambda_1^2)} - \frac{\left[L_{n_1}(J^2+\omega^2L_{n_1})+J^2N_{A_1}\right]}{J^2+\omega^2L_{n_1}^2}R_{n_1} - \frac{\left[L_{n_2}(J^2+\omega^2L_{n_2})+J^2N_{A_2}\right]}{J^2+\omega^2L_{n_2}^2}R_{n_2} \tag{38}$$

and

$$\Delta_2 = \frac{J^2}{a^2p_r} + \frac{JL_{n_1}(L_{n_1}+N_{A_1}-1)}{J^2+\omega^2L_{n_1}^2}R_{n_1} + \frac{J^2(1-J\lambda_1)}{a^2(1+\omega^2\lambda_1^2)} + \frac{JL_{n_2}(L_{n_2}+N_{A_2}-1)}{J^2+\omega^2L_{n_2}^2}R_{n_2}. \tag{39}$$

By comparing the real and imaginary parts of (37), we obtained the oscillatory thermal Rayleigh number

$$R_a^{osc} = -\frac{J\omega^2}{a^2p_r} + \frac{(-J+\pi^2)R_e}{J} + \frac{J^2(J+\omega^2\lambda_1)}{a^2(1+\omega^2\lambda_1^2)} - \frac{\left[L_{n_1}(J^2+\omega^2L_{n_1})+J^2N_{A_1}\right]}{J^2+\omega^2L_{n_1}^2}R_{n_1} - \frac{\left[L_{n_2}(J^2+\omega^2L_{n_2})+J^2N_{A_2}\right]R_{n_2}}{J^2+\omega^2L_{n_2}^2} \tag{40}$$

with the general polynomial form of the equation under study

$$a_1\omega^6 + a_2\omega^4 + a_3\omega^2 + a_4 = 0 \tag{41}$$

where

$$\begin{aligned}
a_1 &= J^2L_{n_1}^2L_{n_2}^2\lambda_1^2, \\
a_2 &= J\Big[a^2L_{n_1}L_{n_2}^2(N_{A_1}-1)p_rR_{n_1}\lambda_1^2 + J^3L_{n_2}^2\lambda_1^2 + L_{n_1}^2\Big(a^2L_{n_2}(N_{A_2}-1)p_rR_{n_2}\lambda_1^2 + J^3\lambda_1^2 \\
&\quad + L_{n_2}^2\big[J+p_r\big(J-J^2\lambda_1+a^2(R_{n_1}+R_{n_2})\lambda_1^2\big)\big]\Big)\Big], \\
a_3 &= J\Big[a^2L_{n_1}\left(N_{A_1}-1\right)p_rR_{n_1}\left(L_{n_2}^2+J^2\lambda_1^2\right) + L_{n_1}^2\Big(J^3+p_r\big[J^3-J^4\lambda_1 \\
&\quad + a^2\big(L_{n_2}\big(L_{n_2}R_{n_1}+(L_{n_2}+N_{A_2}-1)R_{n_2}\big)+J^2R_{n_1}\lambda_1^2\big)\big]\Big) + J^2\Big(a^2L_{n_2}(N_{A_2}-1)p_rR_{n_2}\lambda_1^2 + J^3\lambda_1^2 \\
&\quad + L_{n_2}^2\big[J+p_r\big(J-J^2\lambda_1+a^2R_{n_2}\lambda_1^2\big)\big]\Big)\Big] \\
a_4 &= J^3\Big[J^3+p_r\big[a^2\big(L_{n_1}(L_{n_1}+N_{A_1}-1)R_{n_1}+L_{n_2}(L_{n_2}+N_{A_2}-1)R_{n_2}\big)+J^3(1-J\lambda_1)\big]\Big].
\end{aligned} \tag{42}$$

6.2. Stationary convection

The initiation of stationary convection in the marginal state is determined by substituting $\sigma = 0$ into (36), which provides the thermal Rayleigh number for the non-oscillatory mode, R_a^s, expressed as

$$R_a^s = \frac{\left(a^2+\pi^2\right)^3}{a^2} - (L_{n_1}+N_{A_1})R_{n_1} - \frac{a^2 R_e}{a^2+\pi^2} - (L_{n_2}+N_{A_2})R_{n_2}. \tag{43}$$

From (43), it is apparent that R_a^s depends on non-dimensional parameters: a, L_{n_1}, N_{A_1}, R_{n_1}, R_e, L_{n_2}, N_{A_2} and R_{n_2}. Let us now consider two special cases.

Case I: For nanofluid without electric field (when $R_e = 0$), (43) reduces to

$$R_a^s = \frac{\left(a^2+\pi^2\right)^3}{a^2} - (L_{N_1}+N_{A_1})R_{N_1} - (L_{N_2}+N_{A_2})R_{N_2}, \tag{44}$$

which resembles with earlier result [20].

Case II: For rheological regular fluid (when $L_{n_1}=N_{A_1}=R_{n_1}=L_{n_2}=N_{A_2}=R_{n_2}=0$), (44) reduces further to

$$R_a^s = \frac{\left(a^2+\pi^2\right)^3}{a^2}, \tag{45}$$

which coincides with the prior result [29].

Differentiating (43), we get

$$\frac{\mathrm{d}R_a^s}{\mathrm{d}R_e} = -\frac{a^2}{(a^2+\pi^2)}, \tag{46}$$

$$\frac{\mathrm{d}R_a^s}{\mathrm{d}L_{n_1}} = -R_{n_1}, \tag{47}$$

$$\frac{\mathrm{d}R_a^s}{\mathrm{d}N_{A_1}} = -R_{n_1} \tag{48}$$

$$\frac{\mathrm{d}R_a^s}{\mathrm{d}R_{n_1}} = -\left(N_{A_1}+L_{n_1}\right), \tag{49}$$

$$\frac{\mathrm{d}R_a^s}{\mathrm{d}L_{n_2}} = -R_{n_2}, \tag{50}$$

$$\frac{\mathrm{d}R_a^s}{\mathrm{d}N_{A_2}} = -R_{n_2}, \tag{51}$$

$$\frac{\mathrm{d}R_a^s}{\mathrm{d}R_{n_2}} = -\left(N_{A_2}+L_{n_2}\right). \tag{52}$$

From (46), it is evident that the derivative of its expresion with respect to R_e is negative across all wave numbers, indicating that R_e exerts a destabilizing effect on the system. For nanoparticles with bottom–heavy or top–heavy distributions (corresponding to negative or positive values of R_{n_1} and R_{n_2}), both the nanofluid Lewis numbers L_{n_1} and L_{n_2} and the modified diffusivity ratios N_{A_1} and N_{A_2} contribute to the stabilization or destabilization of the system, as indicated by (48) and (51). Furthermore, in the context of the concentration Rayleigh number, it can be observed from (50) and (52) that the derivatives of their expresions

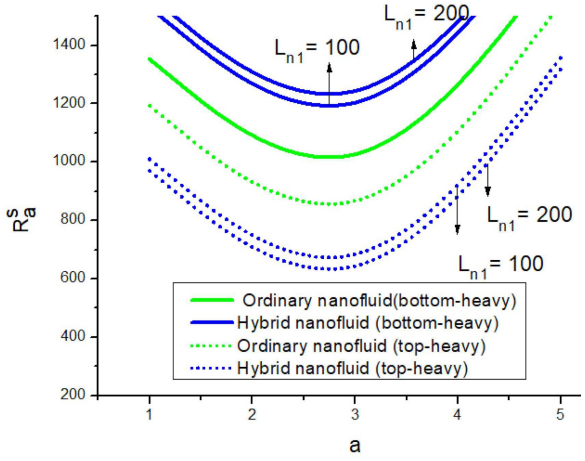

Fig. 2. Effect of L_{n_1} on neutral stability curves in bottom/top–heavy arrangements.

with respect to R_{n_1} and R_{n_2} are consistently negative when $(N_{A_1}+L_{n_1})>0$ and $(N_{A_2}+L_{n_2})>0$, respectively. Typically, for most nanofluids, the values of N_{A_1} and N_{A_2} for both top–heavy and bottom–heavy configurations lie within the ranges $(1 \le N_{A_1}, N_{A_2} \le 10)$ and $(-1 \le N_{A_1}, N_{A_2} \le -25)$, respectively, while the values of L_{n_1} and L_{n_2} are generally in the order of magnitude from 10^3 to 10^6. This suggests that both R_{n_1} and R_{n_2} consistently have a destabilizing effect on the onset of stationary convection. Consequently, the typical parameter ranges indicate that nanoparticle diffusion and buoyancy effects control the onset of convection, providing a means of optimizing thermal transport in applications such as heat exchangers, solar collectors, and electronic cooling.

7. Numerical discussion

The thermal Rayleigh numbers for both oscillatory and stationary modes with stress-free boundaries are given by (40) and (43), respectively. The values are numerically computed using Mathematica 12 software. In the present study, the bottom–heavy and top–heavy configurations refer to the vertical distribution of nanoparticles in the hybrid nanofluid layer. A bottom–heavy arrangement corresponds to a higher concentration of nanoparticles near the lower heated boundary, resulting in a denser base layer. This stabilizes the fluid layer and delays the onset of convection. Conversely, a top–heavy configuration has more nanoparticles near the upper surface, making the top layer denser than the bottom one. This destabilizes the layer, promoting earlier initiation of convective motion. These definitions apply to all fluids, but are particularly amplified in hybrid nanofluids due to the combined effects of multiple nanoparticle types.

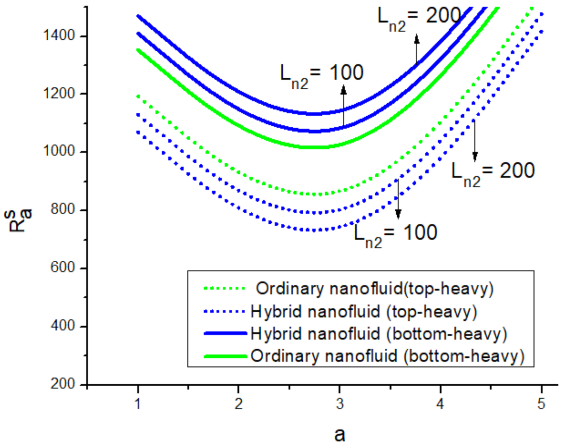

Fig. 3. Effect of L_{N_2} on neutral stability curves in bottom/top–heavy arrangements.

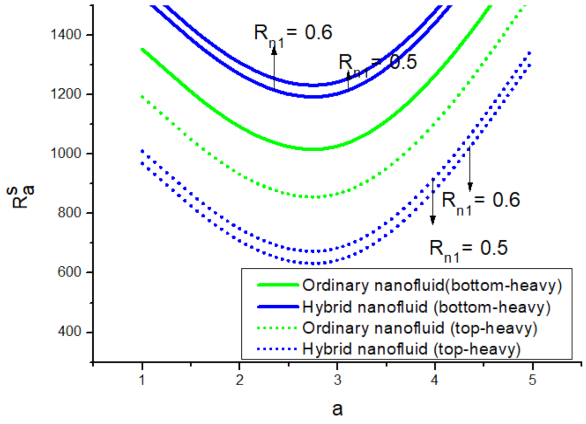

Fig. 4. Effect of R_{n_1} on neutral stability curves in bottom/top–heavy arrangements.

The modified diffusivity ratios N_{A_1} and N_{A_2} and the concentration Rayleigh numbers R_{n_1} and R_{n_2} characterize the vertical distribution of nanoparticles. Negative values indicate a bottom–heavy configuration, where the denser layer resides near the base, enhancing thermal stability and delaying convection. Positive values correspond to a top–heavy distribution, where the denser upper layer destabilizes the fluid, promoting earlier onset of convective. These parameters provide a quantitative measure of the stabilizing or destabilizing effect of nanoparticle stratification. The experimental values for the involved parameters, as provided in [3, 22, 24, 25, 29], are taken as $L_{n_1} = 200$, $N_{A_1} = \pm 3$, $R_{n_1} = \pm 0.4$, $L_{n_2} = 300$, $N_{A_2} = \pm 6$, and $R_{n_2} = \pm 0.6$, $R_e = 100$. To fully understand the stability of convective behaviour in the nanofluid layer, stationary curves are plotted in the R_a^s–a plane.

Figure 2 illustrates the neutral curves for different values of the Lewis number $L_{n_1} = 100, 200$ of the first nanofluid, keeping the other parameters constant. The results reveal a significant trend. As the first nanofluid Lewis number L_{n_1} increases, the stationary Rayleigh number R_a^s decreases. This indicates a crucial impact on convection stability — higher values of this parameter intensify destabilization in a top–heavy distribution, while reinforcing stability in a bottom–heavy distribution. This interplay between thermal diffusion and nanoparticle motion highlights the complex thermodynamic behaviour of hybrid nanofluids in varying configurations.

Moreover, the data reveal a striking contrast. For the top–heavy hybrid nanofluids, the stationary Rayleigh number is significantly lower than that of the ordinary nanofluids, indicating that blending two different nanoparticles can reduce thermal stability compared to a single-nanoparticle system. In contrast, for the bottom–heavy hybrid nanofluids, the stationary Rayleigh number is higher than that of the ordinary nanofluids, suggesting enhanced thermal stability due to the synergistic interaction between multiple nanoparticles. These results confirm that under these conditions, a hybrid nanofluid layer (containing two types of nanoparticles) exhibits greater stability than a single-nanoparticle fluid layer, which is consistent with the observations reported in [20].

For ordinary (single-component) nanofluids, both positive (top–heavy) and negative (bottom–heavy) values of R_{n_1} and R_{n_2} and N_{A_1} and N_{A_2} were used to calculate numerical values, which were then plotted to generate stationary Rayleigh number curves. While generating these curves, the parameters for both nanoparticle types were assumed equal, i.e., $R_{n_1} = R_{n_2}$, $N_{A_1} = N_{A_2}$, $L_{n_1} = L_{n_2}$, to represent a uniform single-nanoparticle system. All other parameters were kept constant across all figures to ensure a consistent and meaningful comparison between ordinary and hybrid nanofluids.

Figure 3 represents the dependence of R_a^s on a for distinct values of the second nanofluid Lewis number, $L_{n_2} = 100$ and 200, in the bottom/top–heavy arrangements. The findings show that an increase in the second nanofluid Lewis number, L_{n_2}, also results in a decrease in the stationary Rayleigh number, R_a^s, for the top–heavy configuration. This confirms a recurring trend that both nanofluid Lewis numbers act as destabilizing agents in the top–heavy distributions while promoting stability in the bottom–heavy configurations. These observations underscore the crucial role of nanoparticle diffusion in shaping the convective behaviour of hybrid nanofluids.

The effects of the first and second concentration Rayleigh numbers, R_{n_1} and R_{n_2}, are examined with respect to nanoparticle distribution (top–heavy and bottom–heavy) and the boundary separation. Figures 4 and 5 illustrate the variation of the stationary Rayleigh number R_a^s with the wave number for various values of $R_{n_1} = 0.5, 0.6$ and $R_{n_2} = 0.5, 0.6$, respectively. For

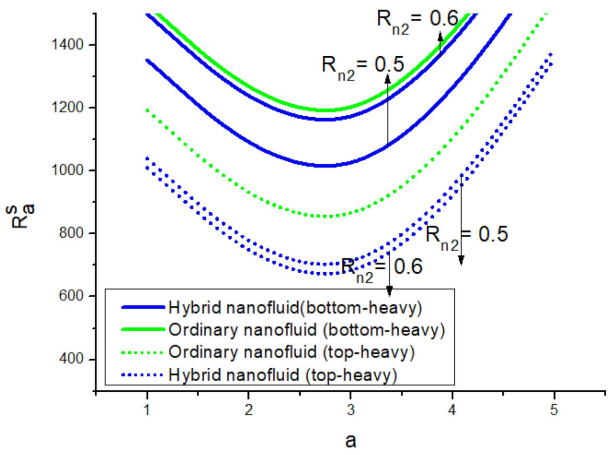

Fig. 5. Effect of R_{n_2} on neutral stability curves in bottom/top–heavy arrangements.

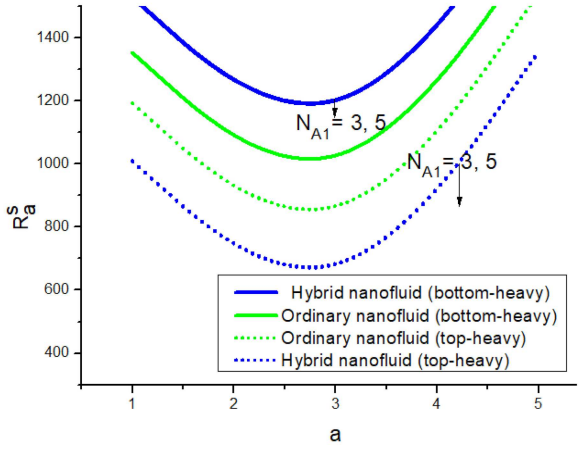

Fig. 6. Effect of N_{A_1} on neutral stability curves in bottom/top–heavy arrangements.

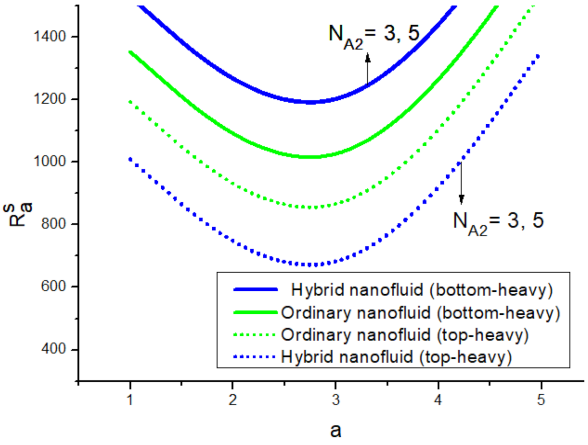

Fig. 7. Effect of N_{A_2} on neutral stability curves in bottom/top–heavy arrangements.

both parameters, a top/bottom–heavy distribution lead to a reduction in the stationary Rayleigh number, indicating a destabilizing effect. In the top–heavy configuration, hybrid nanofluids exhibit a lower stationary Rayleigh number than ordinary nanofluids, indicating that the presence of multiple nanoparticles can destabilize the system and trigger convection earlier. Conversely, in the bottom–heavy arrangement, hybrid nanofluids display a higher stationary Rayleigh number compared to single-component nanofluids, reflecting improved thermal stability arising from the synergistic effect of the two nanoparticle types.

The influence of the modified diffusivity ratios N_{A_1} and N_{A_2} on the onset of stationary convection in hybrid nanofluids is demonstrated in Figs. 6 and 7, respectively, for both top/bottom–heavy nanoparticle distributions. The variations in the diffusivity ratio for $N_{A_2} = 3$ and 5 reveal that the stationary Rayleigh number either increases or decreases depending on the sign and magnitude of N_{A_1}. An increase in N_{A_1} broadens the stability range in bottom–heavy configurations, whereas narrowing the stable regime in top–heavy distributions. Both N_{A_1} and N_{A_2} exhibit similar qualitative trends, affecting the critical conditions for the onset of convection by altering the effective diffusivity of the hybrid nanofluid. Nonetheless, the overall variation in the stability threshold remains modest, suggesting that the modified diffusivity ratios exert only a minor influence on the initiation of stationary convection.

Figure 8 displays the impact of distinct values of electric Rayleigh number, $R_e = 0, 100, 200, 300$, on the stationary thermal Rayleigh number R_a^s as a function of a. The figure indicates a decrement in R_a^s with increasing electric Rayleigh number, which postpones the onset of convection for stationary modes. Hence, the destabilization of a system is depicted by the electric Rayleigh number R_e. This occurs because the electrostatic energy of the physical system increases due to the larger electric field, which makes it less stable in the top/bottom–heavy arrangement of hybrid nanoparticles.

The observed minima in the stationary Rayleigh number curves correspond to critical points where stabilizing forces (viscous resistance and buoyancy) balance destabilizing influences (density differences and thermal gradients). In bottom–heavy configurations, these minima indicate enhanced thermal stability, while in top–heavy configuration, they signify conditions where convection is likely to initiate earlier. The present analysis uncovers a new and physically meaningful observation regarding the convection of an electrically modulated hybrid nanofluid. When an AC electric field is applied, the distribution of nanoparticles within the hybrid nanofluid — whether top–heavy or bottom–heavy — plays a decisive role in determining the onset and intensity of electrohydrodynamic instability. For a top–heavy configuration, where the nanoparticle

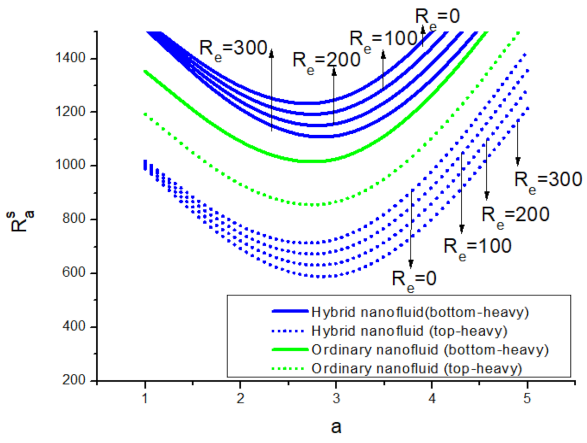

Fig. 8. Effect of R_e on neutral stability curves in bottom/top–heavy arrangements.

concentration is higher near the top boundary, the stationary Rayleigh number decreases, indicating an earlier onset of electroconvective motion. This destabilization occurs because the accumulation of conducting nanoparticles near the top amplifies the local electric field strength and thermophoretic transport, thereby increasing the Maxwell stresses and buoyancy-driven perturbations.

In contrast, for a bottom–heavy configuration, where nanoparticles are concentrated near the bottom boundary, the stationary Rayleigh number increases, demonstrating a stabilizing influence. The combined effects of enhanced effective viscosity, electrical polarization, and nanoparticle layering near the bottom wall suppress perturbation growth and dampen the upward flow. The dual nanoparticle composition further strengthens this stability through differential electrophoretic and dielectrophoretic behavior, which resists electric field-induced flow distortion.

These contrasting effects confirm that electric field-induced convection in hybrid nanofluids is tunable via nanoparticle stratification, providing a controllable electro-thermal mechanism not present in conventional nanofluids. Thus, by manipulating nanoparticle concentration profiles and field intensity, one can achieve either enhanced convective heat transfer — useful in electrohydrodynamic pumps, heat exchangers, and energy systems — or improved thermal stability, advantageous for insulation and microelectronic cooling. This establishes a new coupling mechanism between electric body forces and nanoparticle stratification, forming the theoretical basis for smart, tunable hybrid nanofluid systems capable of adaptive thermal regulation under external electric fields.

A pseudo-homogeneous model was employed, treating the hybrid nanofluid as a single, effective medium with modified thermophysical properties. This approach assumes nanoparticles are well dispersed and move collectively with the base fluid, simplifying the mathematical formulation while accurately capturing the overall thermal and stability behavior. It efficiently incorporates parameters such as concentration Rayleigh numbers, Lewis numbers, and diffusivity ratios, making it suitable for hybrid nanofluid analysis without resorting to complex two-phase particulate modeling.

8. Conclusions

The influence of an AC electric field on a rheological hybrid nanofluid layer is analyzed using the viscoelastic Maxwell model for both top–heavy and bottom–heavy nanoparticle distributions. The findings reveal that:

- Hybrid nanofluids exhibit contrasting thermal stability depending on particle arrangement. In top–heavy configurations, the system is less stable compared to single-particle nanofluids, whereas bottom–heavy distributions of paraticles enhance stability due to the denser base layer suppressing convective motion.
- In top–heavy arrangements, the Lewis number of the nanofluids enhances instability of the system, whereas in bottom–heavy setups it acts as a stabilizing parameter. Modified diffusivity ratios follow a similar qualitative pattern, although their impact on the onset of convection is relatively small. The concentration Rayleigh number consistently promotes instability in both types of particle distributions. Furthermore, the electric Rayleigh number decreases the critical threshold for stationary convection, highlighting its destabilizing influence as a result of increased electrostatic energy in the system.
- Overall, this study provides novel insights into the coupled effects of particle distribution, diffusion, and electric field on hybrid nanofluid stability, offering practical guidance for optimizing nanoparticle selection, concentration, and field parameters in thermal management and microfluidic applications. The results underscore the importance of tailoring nanoparticle arrangements to achieve desired stability characteristics, enabling enhanced control over convective transport and heat transfer performance in advanced hybrid nanofluid systems.

References

[1] H. Bénard, *Rev. Gen. Sci. Pures Appl.* **11**, 1261 (1900).

[2] M.J. Gross, J.E. Porter, *Nature* **212**, 1343 (1966).

[3] P.H. Roberts, *Q. J. Mech. Appl. Math.* **22**, 211 (1969).

[4] A. Castellanos, M.G. Velarde, *Phys. Fluids* **24**, 1784 (1981).

[5] R. Bradley, *Q. J. Mech. Appl. Math.* **31**, 381 (1978).

[6] M. Takashima, H. Hamabata, *J. Phys. Soc. Jpn.* **53**, 1728 (1984).

[7] F. Pontiga, A. Castellanos, *Phys. Fluids* **6**, 1684 (1994).

[8] B. Straughan, *The Energy Method, Stability, and Nonlinear Convection*, Vol. 91, Springer, 2013.

[9] O. Nekrasov, B. Smorodin, *Mathematics* 11, 1188 (2023).

[10] S.U.S. Choi, in: *Proc. of the ASME 1995 Int. Mechanical Engineering Congress and Exposition. Developments and Applications of Non-Newtonian Flows San Francisco, CA*, ASME 1995 p. 99.

[11] J.C. Maxwell, *A Treatise on Electricity and Magnetism*, Vol. 1, Clarendon Press, Oxford 1873.

[12] Y. Xuan, Q. Li, W. Hu, *AIChE J.* **49**, 1038 (2003).

[13] J. Buongiorno, *J. Heat Transf.* **128**, 240 (2006).

[14] D.Y. Tzou, *Int. J. Heat Mass Transf.* **51**, 2967 (2008).

[15] K.V. Wong, O.D. Leon, *Adv. Mech. Eng.* **2**, 1 (2010).

[16] D. Yadav, J. Lee, H.H. Cho, *J. Appl. Fluid Mech.* **9**, 2123 (2016).

[17] I. Saad, S. Maalej, M.C. Zaghdoudi, *Therm. Sci. Eng. Prog.* **16**, 100426 (2020).

[18] G. Huminic, A. Huminic, *Int. J. Heat Mass Transf.* **119**, 813 (2018).

[19] S. Salman, A.R. Abu Talib, S. Saadon, M.T.H. Sultan, *Powder Technol.* **363**, 448 (2020).

[20] V. Kumar, M.K. Awasthi, *SN Appl. Sci.* **2**, 380 (2020).

[21] T. Gul, A. Khan, M. Bilal, N.A. Alreshidi, S. Mukhtar, Z. Shah, P. Kumam, *Sci. Rep.* **10**, 8474 (2020).

[22] S.K. Pundir, M.K. Awasthi, V. Kumar, *J. Nanofluids* **11**, 296 (2022).

[23] M. Sarfraz, M. Yasir, M. Khan, *Nanoscale Adv.* **5**, 6695 (2023).

[24] V. Sharma, A. Chowdhary, U. Gupta, *J. Appl. Fluid Mech.* **11**, 765 (2018).

[25] J. Devi, V. Sharma, A. Thakur, G.C. Rana, *Heat Transf.* **51**, 7787 (2022).

[26] P. Francis, P. Sambath, S. Noeiaghdam, U. Fernandez-Gamiz, S. Dinarvand, *Eng. Sci. Technol. Int. J.* **63**, 101970 (2025).

[27] G.C. Rana, R. Chand, V. Sharma, *Bull. Pol. Acad. Sci. Tech. Sci.* **64**, 143 (2016).

[28] P.K. Gautam, G.C. Rana, H. Saxena, *J.Nanofluids* **12**, 699 (2023).

[29] V. Sharma, J. Devi, G.C. Rana, *J. Taibah Univ. Sci.*, 17, 2229087 (2023).

[30] A.M. Galal, A.M. Obalalu, A.O. Akindele, U. Khan, A.A. Usman, O.A. Olayemi, N.S. Khashi, *Comput. Model. Eng. Sci.* **142**, 3089 (2025).

[31] A. Zeeshan, M.A. Yousif, M.I. Khan, M.A. Latif, S.S. Ali, P.O. Mohammad, *Energies* **18**, 1660 (2025).

[32] S. Chandrasekhar, *Hydrodynamics and Hydromagnetic Stability*, Oxford University Press, 1961.

[33] L.D. Landau, E.M. Lifshitz, *Electrodynamics of Continuous Media*, Pergamon Press, 1960.